PORT SAID ENGINEERING RESEARCH JOURNAL
Faculty of Engineering - Port Said University
Volume 26 No. 2 pp: 146-159

Numerical Analysis of Full Deformation Behavior Study of Pipes Material Using Ring Elongation Testing Technique

*Mahmoud H. Sultan[1, *], Gamal A. Ibrahim[2], Ahmed E. Nassef[3]*

[1] *Production Engineering and Mechanical Design Department, Faculty of Engineering, Port Said University, Port Said, Egypt, email: mahmoud.sultan@eng.psu.edu.eg*

[2] *Production Engineering and Mechanical Design Department, Faculty of Engineering, Port Said University, Port Said, Egypt, email: gamal_osmun@yahoo.com*

[3] *Production Engineering and Mechanical Design Department, Faculty of Engineering, Port Said University, Port Said, Egypt, email: nassef12@eng.psu.edu.eg*

* *Mahmoud H. Sultan, mahmoud.sultan@eng.psu.edu.eg, DOI: 10.21608/PSERJ.2022.126849.1171*

Received 25-3-2022
Revised 13-4-2022
Accepted 20-4-2022

ABSTRACT

This study presents intensive numerical analyses of the ring elongation testing technique (RETT) used to characterize the 7175-T7351 aluminum alloy and St 37 carbon steel rings materials. Theoretical solutions were developed to predict the elastic properties of the materials of the ring using both curved and straight beam formulas. Besides, to predict the full deformation behaviors of the ring's materials, elastic, and elastic-plastic finite element analyses (FEA) were performed on the 2D and 3D ring models. Moreover, FEA were conducted to study the effects of ring dimensions, pin diameter, and ring shape on the RETT results. Modeling the ring specimens with plane stress elements and 3D-stress elements was done with the FEA commercial package (ABAQUS). Theoretical and the FEA results were then compared to the experimental results. The theoretically obtained elastic results accurately predicted the elastic properties of the ring materials. Furthermore, the FEA results successfully predicted the full deformation behaviors of the ring materials.

Keywords: Ring elongation test; non-conventional testing; finite element method; hoop stress; curved beams

1. INTRODUCTION

Mineral tubes and pipes are employed in a variety of engineering areas, including automotive, chemicals, nuclear, and petroleum industries. As a result, the manufacturing processes and applications of those tubes necessitate a thorough understanding of the mechanical properties of their materials. This would aid in the development of proper designs and the safe operation of systems. Because of the anisotropy of tubular materials, their mechanical properties can differ significantly along the axial and transverse (hoop) directions and should thus be measured separately. Furthermore, since pressurized tubes and pipes are primarily subjected to internal pressure, longitudinal cracks are the most common failure mode. For these reasons, the mechanical behavior of tubular materials in the transverse direction should be obtained [1].

The hoop properties of the tubular materials can be measured using a conventional tensile test (standard tensile test) (e.g. [2]). The ASTM E8/E8M material testing standard specifies procedures for determining the hoop properties of tubular materials. The reduced section specimen is cut from the tube in the hoop direction flattened and then tested [3]. The conventional tensile test is the simplest method of evaluating hoop properties; however, due to flattening introduces a pre-strain on the specimen, this method is only suitable for qualitative studies of hoop response [4]. Moreover, the conventional tensile test necessitates the use of specimens with large dimensions. This could be an issue with some materials, such as irradiated material, where only a limited amount of material is available for such tests [5].

Besides conventional tensile tests, non-conventional testing techniques can be employed to measure the hoop properties of the tubular materials such as ring flattening test (e.g. [6–8]), cone-wedge-ring expansion (e.g. [9, 10]), tube-end flaring (e.g. [11, 12]) and tube-inflation

under internal pressure and axial load (e.g. [13–15]). Nevertheless, each of these testing techniques has its own set of limitations.

In addition to the previously mentioned non-conventional testing techniques, there is the ring hoop tension test (RHTT) (e.g. [16–18]). RHTT is typically performed with a ring specimen cut from a pipe or tube and placed over two mandrels that are moved apart by applying axially concentrated load with a universal testing machine. As a result, the ring specimen is elongated in the transverse direction. The specimen can be a full ring (ring without reduced section) (e.g. [19]) or a ring with one or two reduced sections (dog bone-shaped ring) (e.g. [20]). The advantages of using RHTT are its simplicity and feasibility since it is similar to the standard simple tensile test and RHTT requires a minimal amount of material for specimen preparation. Furthermore, the testing apparatus is relatively inexpensive. As a result of these advantages, the RHTT is one of the most important and appealing techniques for assessing the hoop properties of pressure tubes and pipes accurately and consistently [1].

Based on the shape of the loading tool, RHTT can be categorized into two techniques: split-disc testing technique (SDTT) and ring elongation testing technique (RETT). In SDTT, the ring specimen is placed over two D-shaped blocks, whereas in RETT, the ring specimen is elongated using two cylindrical or semi-cylindrical small pins. The ASTM D2290-19a material testing standard specifies the split-disc testing technique for determining the tangential yield and tensile strength of thermoplastic pipes [21]. The main challenge of using the SDTT is the effect of high friction generated during the test between the two D-shaped blocks and the ring specimens' inner surfaces. This friction influences the test results by shifting the global response load versus displacement upward. As a result, obtaining an accurate stress-strain curve of the tubular materials may be difficult [1]. Therefore, several researchers (e.g. [17, 22, 23]) have investigated the effect of friction during SDTT, whereas others (e.g. [1, 18]) have attempted to overcome that friction.

The ISO 8496 material testing standard specifies RETT to reveal surface and internal defects of tubes, as well as to assess the ductility of tubular materials. According to ISO 8496, ring specimen dimensions were restricted to a minimum outside diameter of 150 mm and a minimum thickness of 40 mm [24]. Nonetheless, as previously mentioned, in many cases, only a limited amount of material is available for testing. Therefore, several researchers (e.g. [19]) used the same ISO 8496 testing procedures on ring specimens with small dimensions. Friction is not an issue in RETT since the contact surfaces of the ring specimens' inner surfaces and the two pins are significantly small; thus, the friction generated during the RETT is minimal and can be negligible Furthermore, the clear advantages of using RETT are that the great quantifiable deformation outcomes in a slight strain and that its loading tool can be used with any ring specimen dimensions. However, obtaining an accurate stress-strain curve of the tubular materials using RETT may be difficult because the bending moment developed in the two middle sections of the ring specimen at the start of the test also shifts the global response load versus displacement upward [25].

Few researchers have previously addressed this issue and attempted to measure the hoop properties of tubular materials experimentally. Arsene and Bai proposed reducing bending by elongating a ring specimen with two reduced sections in the hoop direction using a three-part loading tool. The third part is an intermediate piece called dog bone that is inserted between the top and bottom mandrels to prevent the ring specimen' narrowed section from flattening. However, the frictional forces were significantly increased because the contact surface between the specimen and the dog bone was increased. The authors compared finite element analyses (FEA) to their experiments to study the friction effect between the mandrels and the ring specimen's inner surfaces on the stress-strain curves of the Al-Si alloy and Zircaloy material. They found that hoop stress response was influenced by friction and mandrels geometry [25, 26].

Walsh and Adams presented a quadrant ring test technique (QRTT) for overcoming bending in-ring specimens cut from carbon fiber composite pipe by elongating full rings with a loading tool divided into four internal quadrant mandrels. Using FEA, they revealed that the QRTT produced a more uniform stress distribution in the specimen than the SDTT. Nonetheless, due to the small rotation of the fixture quadrants during loading, the tensile strengths obtained using the QRTT were significantly lower than those obtained from conventional tensile testing of flat specimens. Therefore, this fixture arrangement is difficult to work properly. As a result, this fixture arrangement is difficult to work properly [27]. Martín-Rengel et al [28], designed mandrels that consisted of four pieces to overcome bending developed in the notched ring specimen during RHTT of irradiated cladding materials. They used FEA to simulate the RHTT using 3D models with a friction coefficient was assumed to be equal to 0.125 with no justification for their selection, even though, they stated that the RHTT is quite susceptible to this parameter.

By combining experiments and FEA, Kazakeviciute et al [29] used RETT to assess the hoop stress-strain relationship of small ring specimens cut from a 7175-T7351 aluminum pipe. However, they assumed that the ring specimen is a thin beam with constant stress throughout the ring thickness, and these assumptions are only valid for elastic deformation. Finally, Saber and Ali utilized RETT to obtain the mechanical behavior of St 37 carbon steel pipe experimentally. They successfully obtained the yielding load, yield strength, and young's modulus of the pipe material. However, the yield strength was obtained with a large error of about 10.3 percent when compared to the conventional axial tensile

test. Furthermore, they used the trial-and-error method to determine the young's modulus of the pipe material [30].

The current study proposes numerical studies of the RETT to predict the elastic and full deformation behavior of tubular materials. The elastic theoretical solution represented by the curved and straight beam formulas is used to predict the elastic properties of tubular materials. The rings are modeled in 2D and 3D using the FEA commercial package (ABAQUS) to assess the full deformation behaviors of the tubular materials. Furthermore, to investigate the effects of ring dimensions, pin diameter, and ring shape on RETT results. Following that, the theoretical and FEA results compare to the experimental results. The current study has the main advantage of being able to provide accurate and direct numerical techniques for determining the mechanical properties of tubular materials.

2. ANALYTICAL MODELING

2.1. Elastic displacements

The elastic displacement developed in the ring by applying load during the ring elongation testing technique (RETT) can be calculated using both curved and straight beam formulas [30]. In general, both formulas can be determined using the energy method in conjunction with Castigliano's theorem. Figure 1 (a) shows a ring model with the dimensions and a central load P. Because of the symmetry of the geometry and the loading of the ring, the displacement of each quadrant of the ring is identical. As a result, only one quadrant of the ring is considered, as shown in Figure 1 (b). The ring's elastic displacements are given by the relationships [31],

$$\delta_{1,2} = \frac{\partial U_{1,2}}{\partial P} \quad (1)$$

Where δ_1 and δ_2 are the elastic displacements of one quadrant of the ring (mm) using the curved and straight beam formulas, respectively, P is the applied load (N), and U_1 and U_2 are the total strain energy for the ring (N.mm) using the curved and straight beam formulas, respectively, and are defined as:

$$U_1 = U_s + U_N + U_{M1} + U_{MN} \quad (2)$$

$$U_2 = U_{M2} \quad (3)$$

Where U_s, U_N, U_{M1}, U_{MN} and U_{M2} are the strain energy components (N.mm) resulting from the Shear force, the normal force, the bending moment for the curved beam formula, the coupling of the bending moment and the normal force, and the bending moment for the straight beam formula respectively. Since the bending moment and normal force have the same sign in the ring model, U_{MN} is neglected due to its negative sign. The strain energy components can be computed as follows:

$$U_S = \int \frac{kV^2R}{2AG}\, d\theta \quad (4)$$

$$U_N = \int \frac{N^2R}{2AE}\, d\theta \quad (5)$$

Where V is the internal shear force (N) and it is given by $\left(V = \frac{P}{2}\sin\theta\right)$ as shown in Figure 1 (b). θ is the angle from applied load P (degree). R is the distance from the center of curvature of the ring to the ring cross-section

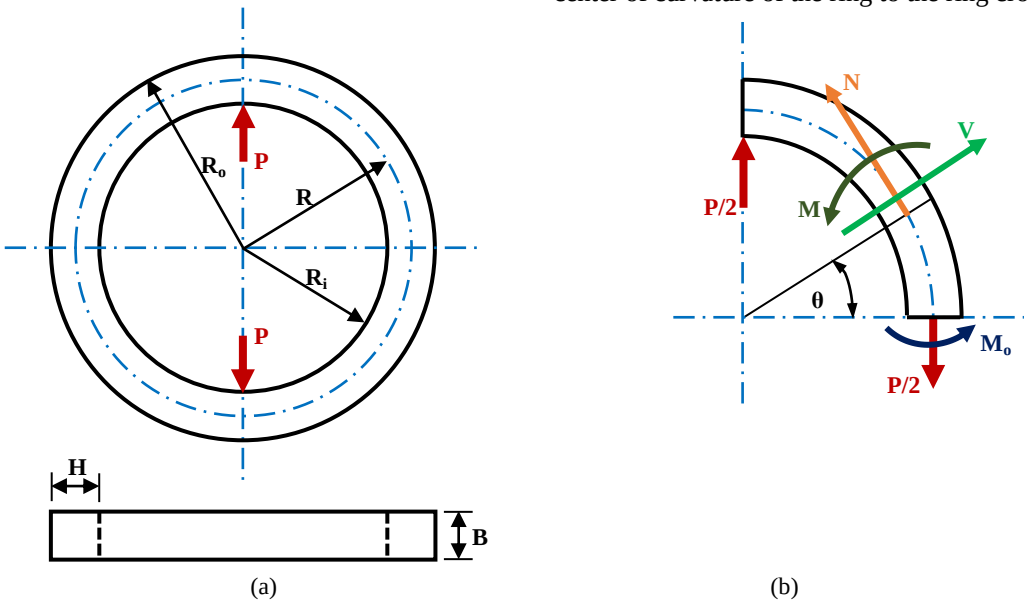

(a) (b)

Figure 1: The ring model's free-body diagram: (a) the full ring model with loading and dimensions and (b) the model of one-quadrant of the ring with the internal loading

centroid (mm) as shown in Figure 1 (a). k is the shear coefficient which equals 1.2 for rectangular cross-sections. A is the cross-sectional area of the ring (mm^2). G is the shear modulus of the ring's material (MPa). N is

the normal traction force (N) and equals to $\left(\frac{P}{2}\cos\theta\right)$ as shown in Figure 1 (b). E is the young's modulus of the ring's material (MPa).

$$U_{M1} = \int \frac{A_m M^2}{2AE(RA_m - A)}\, d\theta \tag{6}$$

$$U_{M2} = \int \frac{M^2 R}{2EI}\, d\theta \tag{7}$$

Where A_m is the parameter has the dimension of length (mm) and equals $\left(B\ln\frac{R_o}{R_i}\right)$ for rectangular cross-section, where B is the width of the ring (mm), R_i and R_o are the inner and outer radius of the ring (mm) respectively as shown in Figure 1 (a). I is the area moment of inertia (mm^4) which equals to $\left(\frac{BH^3}{12}\right)$ for rectangular cross-section. M denotes the moment at angle θ (N.mm) and it is defined as $\left(M = M_{o1,2} - \frac{PR}{2}(1-\cos\theta)\right)$ as shown in Figure 1 (b), where M_{o1} and M_{o2} are the internal moments at an angle $(\theta = 0)$ (N.mm) for curved and straight beam formulas, respectively. By substituting the above parameters in strain energy components, those components can be expressed as follows:

$$U_S = \frac{kP^2R}{8AG}\int_0^{\frac{\pi}{2}} \left(\frac{1}{2} - \frac{1}{2}\cos 2\theta\right) d\theta \tag{8}$$

$$U_N = \frac{P^2R}{8AE}\int_0^{\frac{\pi}{2}} \left(\frac{1}{2} + \frac{1}{2}\cos 2\theta\right) d\theta \tag{9}$$

$$\begin{aligned} U_{M1} = \frac{A_m}{2AE(RA_m - A)}\int_0^{\frac{\pi}{2}} \Bigg(& M_o^2 \\ & - PRM_o(1-\cos\theta) \\ & + \frac{P^2R^2}{4}\left(\frac{3}{2}\right. \\ & - 2\cos\theta \\ & \left. + \frac{1}{2}\cos 2\theta\right)\Bigg) d\theta \end{aligned} \tag{10}$$

$$\begin{aligned} U_{M2} = \frac{R}{2EI}\int_0^{\frac{\pi}{2}} \Bigg(& M_o^2 - PRM_o(1-\cos\theta) \\ & + \frac{P^2R^2}{4}\left(\frac{3}{2}\right. \\ & - 2\cos\theta \\ & \left. + \frac{1}{2}\cos 2\theta\right)\Bigg) d\theta \end{aligned} \tag{11}$$

Equations (8), (9), (10), and (11) are then integrated, yielding:

$$U_S = \frac{\pi k P^2 R}{32AG} \tag{12}$$

$$U_N = \frac{\pi P^2 R}{32AE} \tag{13}$$

$$\begin{aligned} U_{M1} = \frac{A_m}{2AE(RA_m - A)}\Bigg(& M_o^2\frac{\pi}{2} \\ & - PRM_o\left(\frac{\pi}{2} - 1\right) \\ & + \frac{P^2R^2}{2}\left(\frac{3\pi}{8} - 1\right)\Bigg) \end{aligned} \tag{14}$$

$$\begin{aligned} U_{M2} = \frac{R}{2EI}\Bigg(& M_o^2\frac{\pi}{2} - PRM_o\left(\frac{\pi}{2} - 1\right) \\ & + \frac{P^2R^2}{2}\left(\frac{3\pi}{8} - 1\right)\Bigg) \end{aligned} \tag{15}$$

Since the ring's symmetry requires that no rotation occur at the applied load point, then,

$$\frac{\partial U_{M1}}{\partial M_{o1}} = 0$$

$$\frac{\partial U_{M2}}{\partial M_{o2}} = 0$$

Then, by differentiating Equations (14) and (15),

$$M_{o1} = \frac{PR}{2}\left(1 - \frac{2A}{\pi RA_m}\right) \tag{16}$$

$$M_{o2} = \frac{PR}{2}\left(1 - \frac{2}{\pi}\right) \tag{17}$$

Table 1: Chemical composition (wt.%) of 7175-T7351 aluminum alloy [32] **and St 37 low carbon steel** [33]

Chemical composition of 7175-T7351 aluminum alloy [32]									
Element	Cu	Mg	Si	Fe	Cr	Zn	Mn	Al	
Wt.%	1.2-2	2.1-2.9	0.15	0.2	0.18-0.28	5.1-6.1	0.1	Balance	
Chemical composition of St 37 low carbon steel [33]									
Element	C	Si	P	S	Mn	Ni	Cr	Mo	Fe
Wt.%	0.15	0.073	< 0.008	0.009	0.491	< 0.03	< 0.01	< 0.008	Balance

To obtain the total strain energy for the ring using the curved and straight beam formulas Eqs (12), (13), and (14) are subbed back into Eq. (2), and Eq. (15) is subbed back into Eq. (3) as follows:

$$U_1 = \frac{\pi k P^2 R}{32AG} + \frac{\pi P^2 R}{32AE} + \frac{A_m}{2AE(RA_m - A)}\left(M_o^2 \frac{\pi}{2} - PRM_o\left(\frac{\pi}{2} - 1\right) + \frac{P^2R^2}{2}\left(\frac{3\pi}{8} - 1\right)\right) \quad (18)$$

$$U_2 = \frac{R}{2EI}\left(M_o^2 \frac{\pi}{2} - PRM_o\left(\frac{\pi}{2} - 1\right) + \frac{P^2R^2}{2}\left(\frac{3\pi}{8} - 1\right)\right) \quad (19)$$

The elastic displacements of one quadrant of the ring can be calculated using Eq. (1) by differentiating the total strain energy $U_{1,2}$ concerning the applied load P as:

$$\delta_1 = \frac{\pi k PR}{16AG} + \frac{\pi PR}{16AE} + \frac{A_m}{2AE(RA_m - A)}\left(PR^2\left(\frac{3\pi}{8} - 1\right) - RM_o\left(\frac{\pi}{2} - 1\right)\right) \quad (20)$$

$$\delta_2 = \frac{R}{2EI}\left(PR^2\left(\frac{3\pi}{8} - 1\right) - RM_o\left(\frac{\pi}{2} - 1\right)\right) \quad (21)$$

As previously stated, the elastic displacement of each quadrant of the ring is identical. As a result of using the curved and straight beam formulas, the ring's total elastic displacements (δ_1^*, δ_2^*) using the curved and straight beam formulas, respectively are given by:

$$\delta_1^* = \frac{\pi k PR}{4AG} + \frac{\pi PR}{4AE} + \frac{2A_m}{AE(RA_m - A)}\left(PR^2\left(\frac{3\pi}{8} - 1\right) - RM_o\left(\frac{\pi}{2} - 1\right)\right) \quad (22)$$

$$\delta_2^* = \frac{2R}{EI}\left(PR^2\left(\frac{3\pi}{8} - 1\right) - RM_o\left(\frac{\pi}{2} - 1\right)\right) \quad (23)$$

2.2. Elastic stress

The elastic stress developed in the ring during the RETT can be considered according to polar coordinates (r, θ), owing to the ring curvature nature. The radial stress σ_{rr}, and shear stress $\sigma_{r\theta}$ are sufficiently small. Therefore, the stress state is essentially one-dimensional in the hoop direction. As in the elastic displacement determination, the elastic circumferential stress $\sigma_{\theta\theta}$ developed in the ring can be determined using both curved and straight beam formulas by the relations [31],

$$\sigma_{\theta\theta 1} = \frac{N}{A} + \frac{M(A - rA_m)}{Ar(RA_m - A)} \quad (24)$$

$$\sigma_{\theta\theta 2} = -\frac{My}{I} \quad (25)$$

Where y is the distance from the neutral axis of bending of the cross-section (centroid of the cross-section) to the point in the cross-section at which $\sigma_{\theta\theta 2}$ acts (mm). $\sigma_{\theta\theta 1}$ and $\sigma_{\theta\theta 2}$ are the elastic hoop stresses (MPa) using the curved and straight beam formulas, respectively.

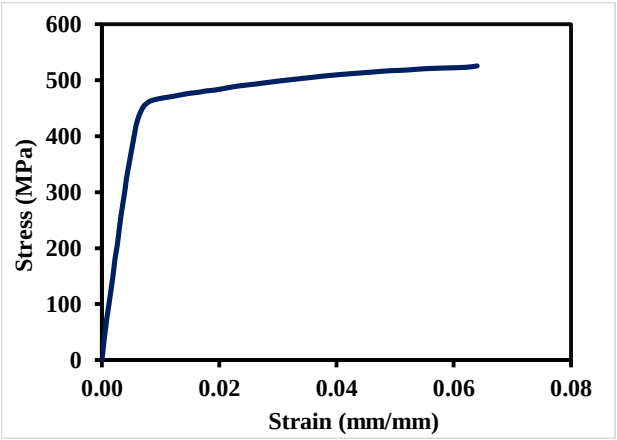

(a)

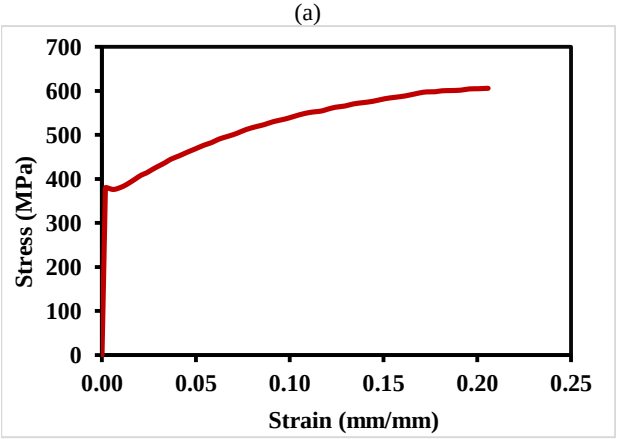

(b)

Figure 2: True stress-strain curve: (a) 7175-T7351 aluminum alloy, reproduced from [29]**, and (b) St 37 low carbon steel, reproduced from** [30]

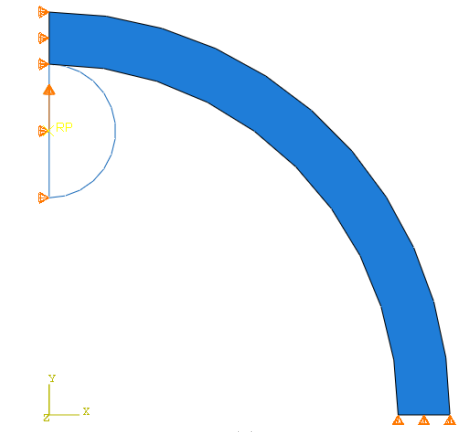

(a)

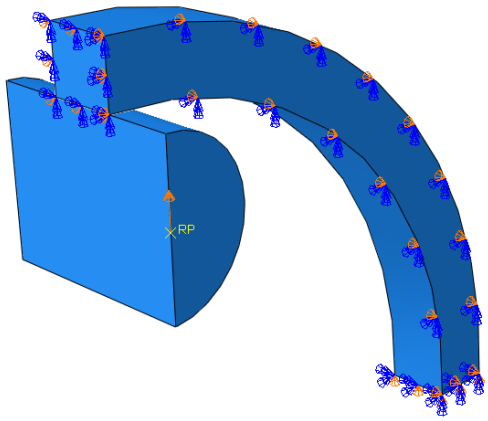

(b)

Figure 3: a quarter St 37 ring model with appropriate load and boundary conditions: (a) 2D FEA model, and (b) 3D FEA model

3. MATERIALS

The materials used in this study for the ring's models were 7175-T7351 aluminum alloy (7175-T7351) and, St 37 low carbon steel (St 37) with the chemical composition and mechanical properties shown in

Table 1 [32, 33] and Figure 4: Mesh in a quarter St 37 ring model: (a) 2D FEA model, and (b) 3D FEA model

Table 2 [29, 30], respectively. The 7175-T7351 is a heat-treated wrought alloy used in aircraft gearbox housing applications and was assumed to be isotropic material [29]. Because of its good heat conductivity and corrosion resistance, St 37 is widely used in industry, including gas pipelines, alloy wheels, and stationary engineering components [34]. The true stress-strain curves at room temperature for 7175-T7351 and St 37 are shown in Figure 2 (a) [29] and Figure 2 (b) [30], respectively.

4. FINITE ELEMENT MODELLING

Since ring models have symmetry in their geometry and loading, 2D and 3D finite element analyses (FEA) were performed on a quarter ring model with appropriate boundary conditions applied to each plane of symmetry, as shown in Figure 3 (a) and Figure 3 (b). The boundary conditions are the same for the St 37 and 7175-T7351 ring models. Table 3 shows the dimensions of the rings and loading pins. To account for the large deformations, ABAQUS/Standard was used to model the rings with geometric non-linearity active during the loading step. Since the stiffness of the pin material is significantly greater than that of the ring material, a discrete rigid body was used to model the loading pin. The loading pin's center was specified as a reference point which was loaded with an upward vertical displacement of 15 mm and 2 mm for the St 37 and 7175-T7351 ring models, respectively. The data from the uniaxial tensile test (true stress-strain data) for St 37 and 7175-T7351 were used to conduct elastic and elastic-plastic FEA.

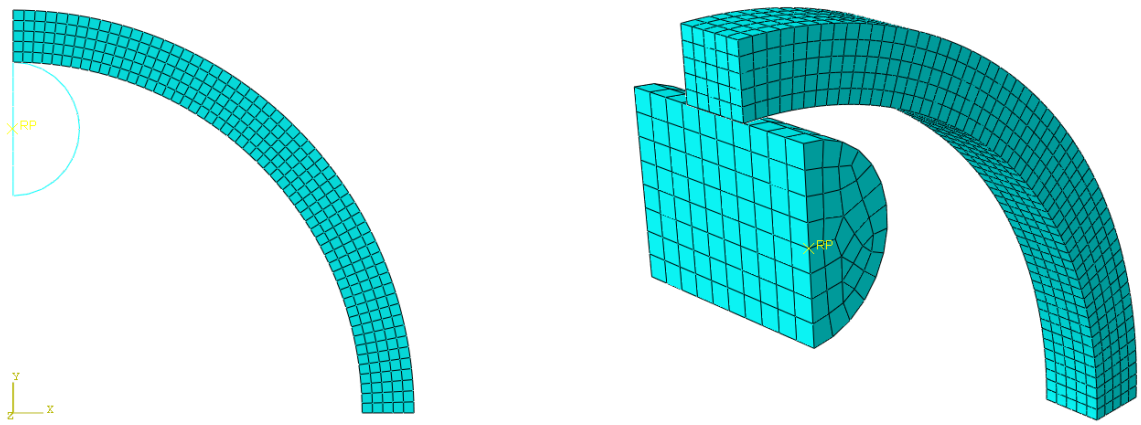

(a) (b)

Figure 4: Mesh in a quarter St 37 ring model: (a) 2D FEA model, and (b) 3D FEA model

Table 2: Mechanical properties of 7175-T7351 aluminum alloy [29] **and St 37 low carbon steel** [30]

Material	Young's modulus (MPa)	Yield strength (MPa)	Poisson's ratio
7175-T7351	72.5×10^3	450	0.3
St 37	210×10^3	380	0.3

Table 3: Dimensions of 7175-T7351 aluminum alloy and St 37 low carbon steel ring models

Ring model	Outer radius (mm)	Inner radius (mm)	Width (mm)	Pin diameter (mm)
7175-T7351	5.5	4.5	2	2.5
St 37	30.15	26.25	4	10

4.1. Mesh sensitivity

Plane stress elements (CPS4R), and 3D stress elements (C3D8R) were used to mesh the ring models, as shown in Figure 4 (a) and Figure 4 (b). A mesh sensitivity study was carried out on the ring models to determine an adequate number of elements across the ring thickness (elements size). For each model with a specific wall thickness, several FEA were carried out using different element sizes. The reaction forces were then normalized and plotted against the number of elements across the ring thickness as shown in Figure 5. It was found that the reaction forces are insensitive to the mesh size when the number of elements across the ring thickness is equal to or greater than five elements. Furthermore, it was found that the element size of the loading pin does not affect the model outputs.

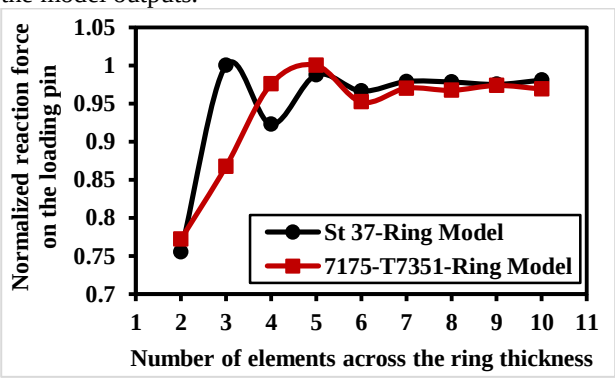

Figure 5: Number of elements across the ring thickness against the reaction force on the loading pin

4.2. Contact

ABAQUS general contact was used to define the contact between the pin and the inner surfaces of the ring. The effect of friction generated between the pin and the ring during the ring elongation testing technique (RETT) on the 7175-T7351 ring model was investigated using different coefficients of friction (μ) of 0, 0.15, 0.3, and 0.5. Figure 6 shows the hoop stress (MPa) at different coefficients of friction for the 7175-T7351 ring model. It can be found that the coefficient of friction had almost no effect on stress, strain, or reaction force on the pin for large deformations. As a result, the model was therefore initialized with a frictionless contact.

5. RESULTS AND DISCUSSION

5.1. Elastic and elastic-plastic behaviors

The experimental results of testing ring specimens, given in [29] and [30] were used to validate the theoretical and FEA results of the 7175-T7351 and St 37 ring models. The elastic behaviors of the ring models were predicted using the curved and straight beam displacement formulas given in Eqs. (22) and (23), respectively. The obtained results were then compared to the experimental results as shown in Figure 7 (a) and Figure 7 (b). Besides, 2D and 3D FEA were used to predict the elastic-plastic behaviors (Full deformation behaviors) of the ring models by extracting the load-displacement responses from the reference point of the

loading pin in the y-direction. Figure 8 (a) and Figure (b) compare the FEA results to experimental results. It can be found that the elastic behaviors predicted by the curved and straight beam displacement formulas agree very well with the experimental elastic results for both models. Moreover,

Table 4: Summary of the numerical values of the parameters used to calculate the yield strength

Ring material	Yielding Load (N)	N (N)	A (mm^2)	M (N.mm)	r (mm)	Am (mm)	R (mm)
7175-T7351	155	0	2	140.339	4.5	0.401	5
St 37	760	0	15.6	3887.766	26.25	0.554	28.2

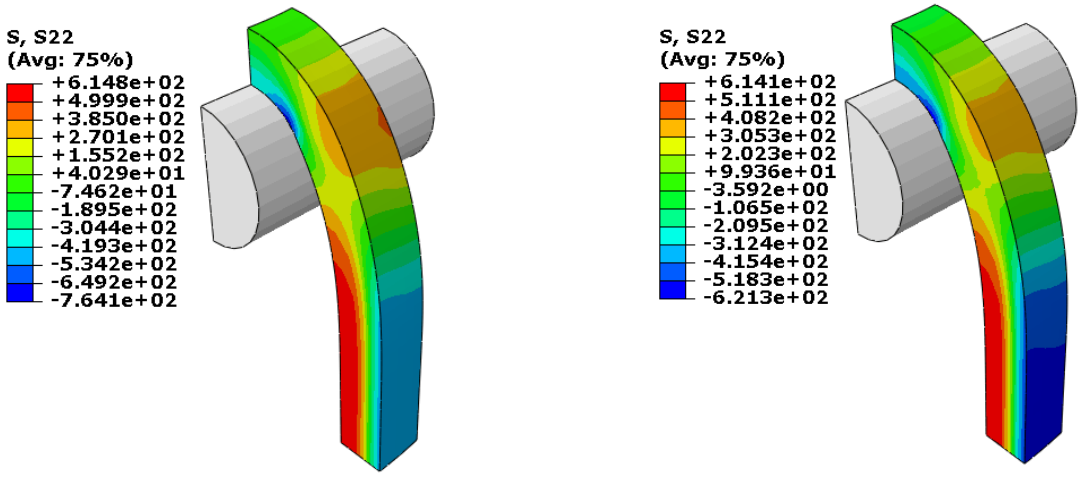

(a) (b)

Figure 6: Hoop stress (MPa) of the 7175-T7351 ring model: (a) μ=0 and (b) μ=0.5

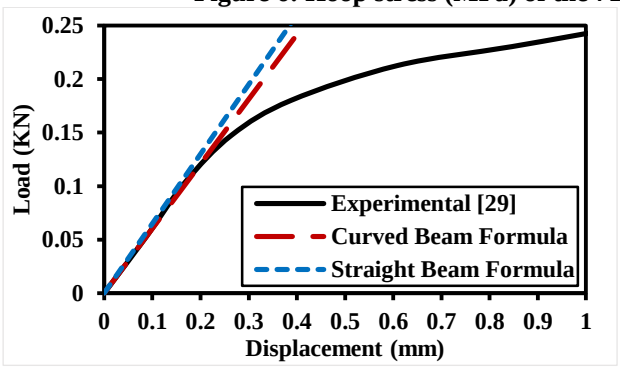

(a)

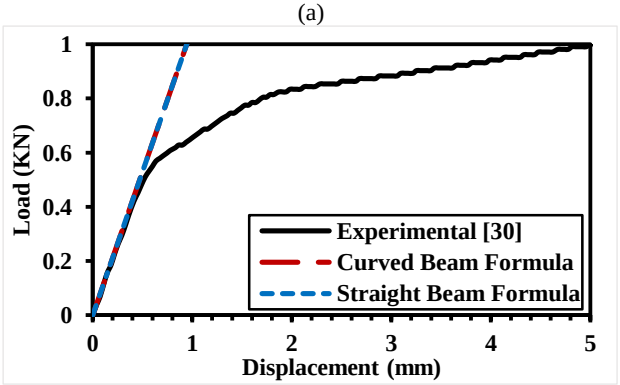

(b)

Figure 7: Curved and straight beam displacement formulas in comparison with the experimental results: (a) 7175-T7351 ring reproduced from [29] **and (b) St 37 ring reproduced from** [30]

the elastic-plastic behaviors predicted by 2D and 3D FEA for both models closely match the experimental elastic-plastic results.

As stated in [30], the yielding load can be obtained directly from the experimental ring elongation testing technique (RETT) results, and it equals 760 N for the St 37 ring. Using the same approach, the yielding load of the 7175-T7351 ring was obtained to be 155 N, as shown in Figure 9. The yield strength of the 7175-T7351 and St 37 ring materials was determined directly from the experimental RETT results using the curved and straight beam stress formulas provided in Eqs. (24) and (25) respectively. Table 4 shows the numerical values of the parameters used to calculate the yield strength of both ring materials. The straight beam displacement formula given in Eq. (23) was also used to determine the young's modulus of the 7175-T7351and St 37 ring materials.

The young's modulus was also calculated directly from the experimental RETT results at the point where the load equals 103.346 (N) and the displacement equals 0.1675 (mm) for the 7175-T7351 ring and the load equals 156.96 (N) and the displacement equals 0.1295 (mm) for the St 37 ring. Table 5 shows the yield strength and young's modulus result obtained for the 7175-T7351 and St 37 ring materials. When compared to the true axial tensile data for the materials, the curved beam stress formula produced an accurate yield strength with an error percentage of 0.21 percent for the 7175-T7351 ring that has a mean radius-to-thickness ratio (R/H) equals 5 as shown in Figure 10. In contrast, the straight beam stress formula produced an accurate yield strength with an error percentage of 1.0417 percent for a St 37

ring with an (R/H) ratio of 7.23 as shown in Figure 10. The young's modulus was successfully obtained using the straight beam displacement formula with an error percentage of 5.1 percent for the 7175-T7351 ring material and 2.62 for the St 37 ring material when compared to the true axial tensile data for the materials as shown in Figure 11.

5.2. The influence of ring dimensions, pin diameter, and ring shape

5.2.1. Ring dimensions

Table 5: The yield strength and young's modulus of the 7175-T7351 and St 37 ring materials

Ring material	Yield strength (MPa) Curved beam formula	Yield strength (MPa) Straight beam formula	Young's modulus (MPa)
7175-T7351	450.95	422.4	68.8×10^3
St 37	401.9	384	204.5×10^3

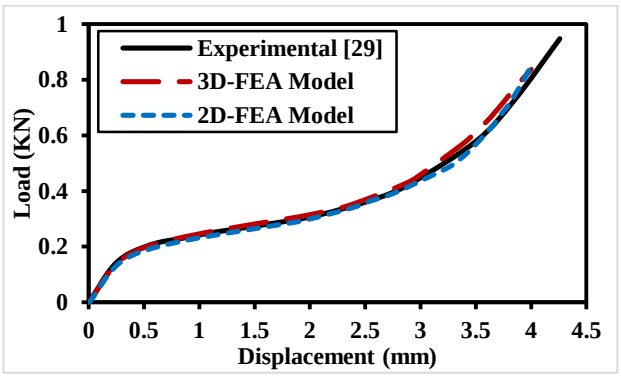

(a)

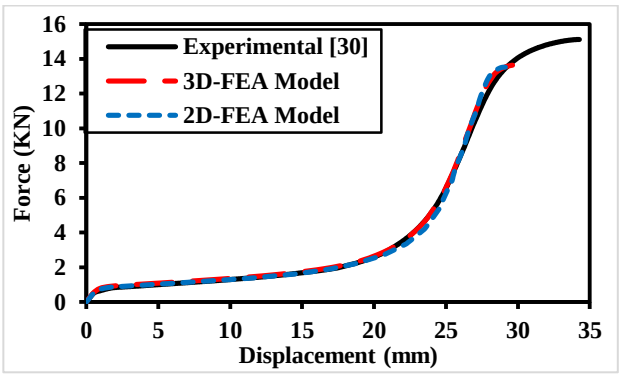

(b)

Figure 8: Elastic-plastic load-displacement responses: (a) 7175-T7351 aluminum alloy ring model and (b) St 37 low carbon steel ring model

FEA were performed on a St 37 ring using 3D ring models to study the effects of the ring's width and thickness on the load-displacement response. Rings with (i) constant thickness and different width values and (ii) constant width and different thickness values were tested. Figure 12 compares the behavior of those rings when modeled using 3D stress elements. It can be seen that for the rings that have the same cross-section area a larger thickness shows a higher loading capacity in the elastic zone. Alternatively, a ring with a larger width shows a larger plastic deformation zone. Rings with the same cross-section area and a width-to-thickness ratio (B/H) between 0.975 and 1.0256 exhibit no difference in load-displacement response. As a result, the correct ring width and thickness must be chosen following that ratio.

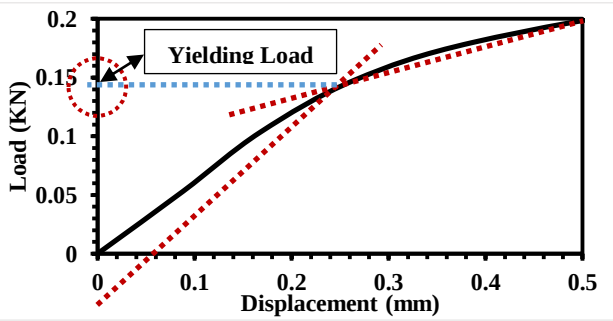

Figure 9: Yielding load of 7175-T7351 aluminum alloy ring material

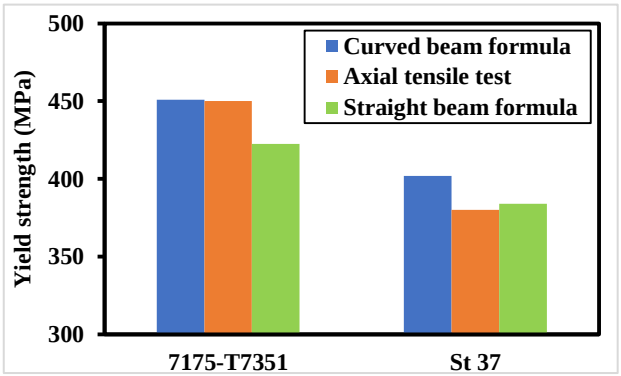

Figure 10: Yield strength values for the 7175-T7351 aluminum alloy ring with (R/H=5) and St 37 low carbon steel ring with (R/H=7.23) ring model obtained theoretically in comparison with that obtained from the axial tensile test

5.2.2. Pin diameter

To investigate the effects of the loading pin diameter on the RETT results, 3D elastic-plastic FEA were performed on a quarter of the St 37 ring model. The loading pin diameters (Dp) used were 5, 10, 15, 20, and 25 mm. All ring models have the same load and boundary conditions. Figure 13 shows the load-displacement responses extracted from the loading pin's reference point in the y-direction for each loading pin diameter. The load-displacement response does not change as the loading pin diameter increases up to a

displacement of 10 mm. However, once the displacement exceeded 10 mm, the load-displacement response shifted to the left and the displacement decreased significantly. Nonetheless, the maximum load difference was minor. As the ring model deforms, it experiences a great deal of bending moments. Models with smaller pin diameters experience more bending than those with larger pin diameters. When small pins are used, the applied load is consumed more to elongate the ring before setting it in a tensile mode. However, using large pins is accompanied by less bending, less elongation, and more tension. However, the friction between the ring and the pin surfaces increases due to the increase in the contact area between the pin and the ring.

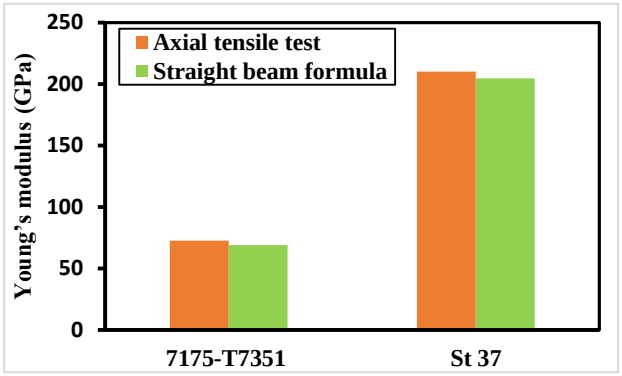

Figure 11: Young's modulus values obtained theoretically for the 7175-T7351 aluminum alloy ring with (R/H=5) and St 37 low carbon steel ring with (R/H=7.23) ring model in comparison with that obtained from the axial tensile test

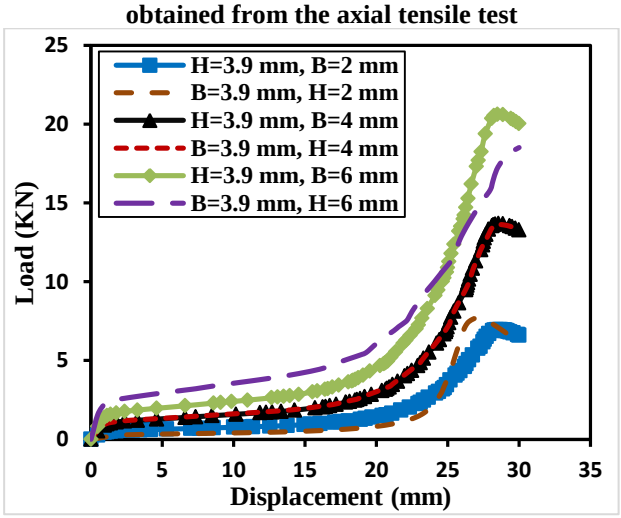

Figure 12: Load displacement for 3D models of rings with (i) constant thickness and varying widths and (ii) constant width and varying thicknesses

Figure 14 shows the equivalent plastic strain in the ring models against the loading pin with different diameters. Because of the concentrated stresses at the loading pin, all of the ring models failed in nearby the loading pin. Furthermore, the high plastic strain zone near the pin caused the ring models to fail prematurely. Furthermore, the high plastic strain zone close to the pin caused the ring models to fail prematurely. The failure zone moves away from the point of impact of the load on the ring with
increasing the loading pin diameter owing to the increase in the contact area. The equivalent plastic strain in a material (PEEQ) is a scalar variable that represents the inelastic deformation of a material. If this variable exceeds zero, the material is yielding [35].

5.2.3. Ring shape

FEA was conducted on the two different shapes of St 37 ring models to overcome the failure of the rings in the vicinity of the loading pin. As shown in Figure 15, the first ring was notched, and the second was a dog bone-shaped ring. The notched and the dog bone-shaped St 37 ring models were subjected to the same FEA procedures as the St 37 full ring model, with no modifications. Figure 16 compares the load-displacement responses of the notched and dog bone-shaped St 37 ring models to the St 37 full ring model. The behaviors of the notched and the dog bone-shaped ring models were found to be in perfect agreement with the behavior of the full ring model. Furthermore, as shown in Figure 17, the rings failed exactly in the center of the rings. As a result, rings can be used in the ring elongation technique to overcome ring specimen failure near the loading pin. Moreover, the dog bone-shaped ring can be used in the RETT to obtain stress-strain data by acquiring gauge length and cross-section area for the ring specimen.

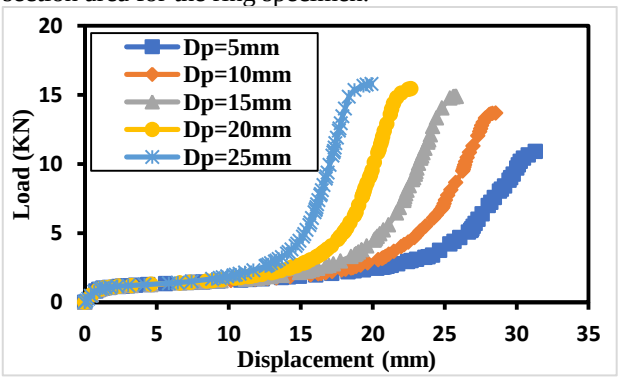

Figure 13: Load-displacement of the ring models with different loading pins diameters

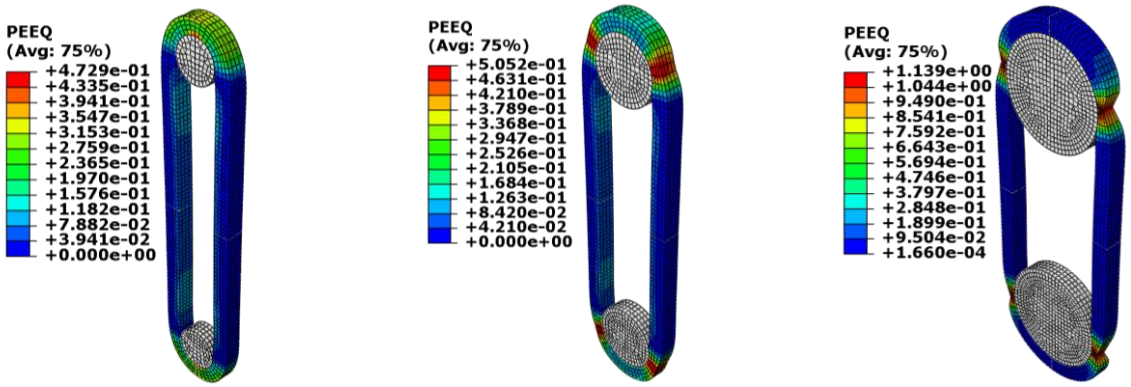

(a) (b) (c)

Figure 14: The equivalent plastic strain in the ring models against the loading pins with different diameters: (a) Dp = 10 mm, (b) Dp = 15 mm, and (c) Dp = 25 mm

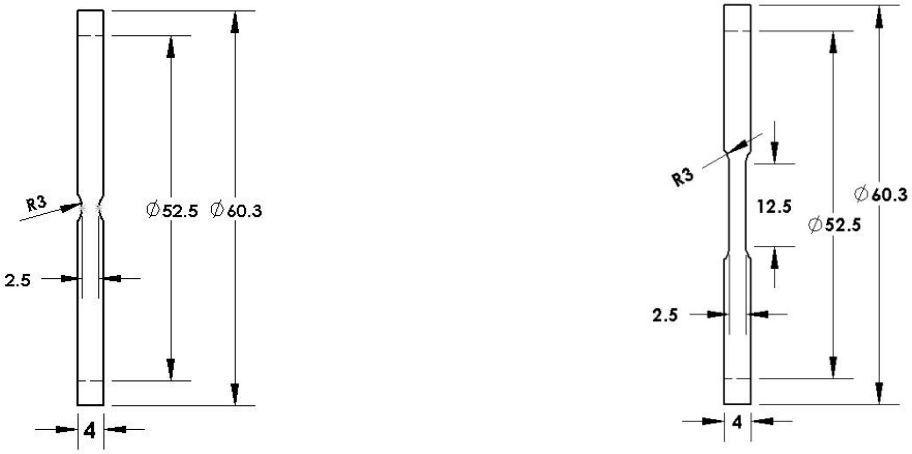

(a) (b)

Figure 15: Dimensions of two different shapes of rings (a) notched ring and (b) dog bone-shaped ring

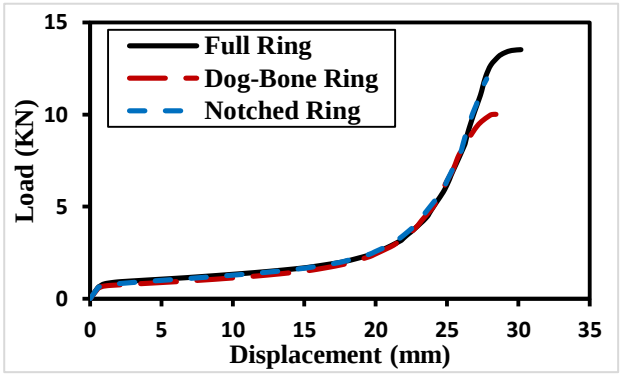

Figure 16: Load-displacement for St 37 notched ring model, St 37 dog bone-shaped ring model, and St 37 full ring model

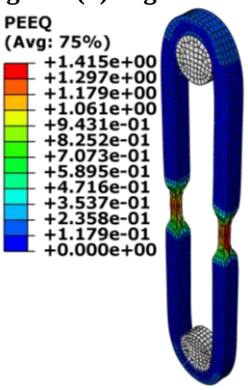

(a)

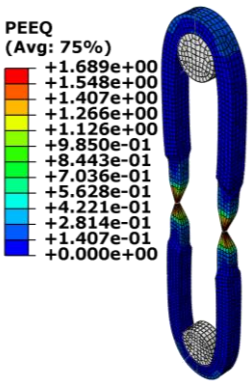

(b)

Figure 17: Equivalent plastic strain in the St 37 ring models: (a) notched ring model and (b) dog bone-shaped ring model

6. CONCLUSIONS

Theoretical and FEA were carried out to study the ring elongation testing technique as the materials characterization testing technique. Theoretical and the FEA results were then compared to the experimental results. Furthermore, FEA were carried out to study the influence of ring dimensions, pin diameter, and ring shape on the RETT results, and the following are some conclusions:

- The curved and straight beam displacement formulas successfully predicted the elastic behaviors of rings with (R/H) equals 5 and 7.23.
- The elastic-plastic behaviors of the rings were correctly predicted by FEA.
- For the 7175-T7351 ring with (R/H) ratio of 5, the yield strength was successfully obtained directly from the RETT experimental results using the curved beam stress formula with an accuracy of 99.79 percent when compared to the true axial tensile data for the material as shown in Figure 10. Therefore, to accurately calculate materials' yield strength using RETT, the curved beam stress formula should be utilized for rings with an (R/H) ratio of 5.
- The yield strength for the St 37 ring with (R/H) ratio of 7.23 was also successfully obtained directly from the RETT experimental results using the straight beam stress formula with an accuracy of 98.958 percent when compared to the true axial tensile data for the material as shown in Figure 10. As a result, the straight beam stress formula must be used with rings that have an (R/H) ratio of 7.23 to determine the accurate yield strength of the materials using RETT.
- When compared to the true axial tensile data for the materials, the young's modulus was successfully obtained directly from the RETT experimental results using the straight beam displacement formula with an accuracy of 94.9 and 97.38 percent for the 7175-T7351 and St 37 ring materials, respectively as shown in Figure 11. Therefore, the straight beam displacement formula can be used with rings with (R/H) ratios ranging from 5 to 7.23 to accurately determine the young's modulus of materials using RETT.
- FEA must be performed to obtain the correct ring's width and thickness for testing using the ring elongation testing technique.
- Pins with small diameters may be selected to minimize the friction between the pins and the inner ring surfaces and to overcome ring prematurely fail.
- Notched ring specimen and dog bone-shaped ring specimen can be used in the ring elongation testing technique to overcome the failure of the ring specimen in nearby the loading pin; besides, the notched ring specimen can be used to attain stress-strain data by acquiring gauge length and cross-section area for the ring specimen.

Credit Authorship Contribution Statement

Mahmoud H. Sultan: Software, Resources, Investigation, Data Curation, &Writing. **Gamal A. Ibrahim**: Conceptualization, Investigation, Formal analysis, Resources, supervision. **Ahmed E. Nassef**: Validation, Writing, supervision, Review & Editing.

Declaration of competing Interest

The authors declare that there is no conflict of interest regarding the publication of this paper.

Declaration of Funding

The authors did not receive support from any organization for the submitted work.

7. REFERENCES

[1] A. Khalfallah, Z. Ktari, C. Leitão, and J. V. Fernandes, "New Mandrel Design for Ring Hoop Tensile Testing," *Exp. Tech.*, vol. 45, no. 6, pp. 769–787, Dec. 2021. https://doi.org/10.1007/s40799-021-00462-4.

[2] T. Zribi, A. Khalfallah, and H. BelHadjSalah, "Experimental characterization and inverse constitutive parameters identification of tubular materials for tube hydroforming process," *Mater. Des.*, vol. 49, pp. 866–877, 2013. https://doi.org/10.1016/j.matdes.2013.02.077

[3] A. Standard, "E8/E8M-13a," *Stand. Test Methods Tens. Test. Met. Mater. ASTM Int. West Conshohocken, PA*, 2013. https://doi.org/10.1520/E0008_E0008M-13A

[4] C. P. Dick and Y. P. Korkolis, "Mechanics and full-field deformation study of the Ring Hoop Tension Test," *Int. J. Solids Struct.*, vol. 51, no. 18, pp. 3042–3057, 2014. https://doi.org/10.1016/j.ijsolstr.2014.04.023

[5] M. Király, D. M. Antók, L. Horváth, and Z. Hózer, "Evaluation of axial and tangential ultimate tensile strength of zirconium cladding

tubes," *Nucl. Eng. Technol.*, vol. 50, no. 3, pp. 425–431, 2018. https://doi.org/10.1016/j.net.2018.01.002

[6] J. Herb, J. Sievers, and H. G. Sonnenburg, "A new cladding embrittlement criterion derived from ring compression tests," *Nucl. Eng. Des.*, vol. 273, no. March, pp. 615–630, 2014. https://doi.org/10.1016/j.nucengdes.2014.03.047

[7] H. M. Tahar, H. Djebaili, and B. Daheche, "Analysis of Control by Flattening of the Welded Tubes," *Int. J. Mater. Metall. Eng.*, vol. 9, no. 11, pp. 1324–1328, 2015. https://doi.org/10.5281/zenodo.1129698

[8] F. J. Gómez, M. A. Martin Rengel, J. Ruiz-Hervias, and M. A. Puerta, "Study of the hoop fracture behaviour of nuclear fuel cladding from ring compression tests by means of non-linear optimization techniques," *J. Nucl. Mater.*, vol. 489, pp. 150–157, 2017. https://doi.org/10.1016/j.jnucmat.2017.03.043

[9] H. Jiang and J.-A. J. Wang, "Development of cone-wedge-ring-expansion test to evaluate the tensile HOOP properties of nuclear fuel cladding," *Prog. Nucl. Energy*, vol. 108, pp. 372–380, 2018. https://doi.org/10.1016/j.pnucene.2018.06.015

[10] M. Saber and H. Chouikhi, "Development of the Bicone Mandrel Ring Expansion Test to Evaluate the Hoop Stress in Extruded Aluminum Tubes," *Experimental Mechanics*, vol. 61, no. 5. pp. 791–802, 2021. https://doi.org/10.1007/s11340-021-00692-y

[11] T. Daxner, F. G. Rammerstorfer, and F. D. Fischer, "Instability phenomena during the conical expansion of circular cylindrical shells," *Comput. Methods Appl. Mech. Eng.*, vol. 194, no. 21-24 SPEC. ISS., pp. 2591–2603, 2005. https://doi.org/10.1016/j.cma.2004.07.047

[12] Z. Sun, J. Cao, L. Huang, Z. Yin, and L. Zheng, "Buckling behavior of AA6061 circular tube under axial compression by considering contact condition of tube end," *Int. J. Light. Mater. Manuf.*, vol. 4, no. 3, pp. 383–392, 2021. https://doi.org/10.1016/j.ijlmm.2021.06.001

[13] Y. P. Korkolis and S. Kyriakides, "Inflation and burst of anisotropic aluminum tubes for hydroforming applications," *Int. J. Plast.*, vol. 24, no. 3, pp. 509–543, Mar. 2008. https://doi.org/10.1016/j.ijplas.2007.07.010

[14] Y. P. Korkolis and S. Kyriakides, "Hydroforming of anisotropic aluminum tubes: Part I experiments," *Int. J. Mech. Sci.*, vol. 53, no. 2, pp. 75–82, 2011. https://doi.org/10.1016/j.ijmecsci.2010.11.003

[15] W. Gowayed, S. Abdou, M. Fouda, and M. Samy, "Technical Feasibility Study of Using Low Carbon Steel pipes in Natural Gas Pipeline Installations in the Egyptian Coastal Areas 'Port Said and Alexandria,'" *Port-Said Eng. Res. J.*, vol. 17, no. 2, pp. 11–17, 2013. https://doi.org/10.21608/pserj.2013.46920

[16] H.-Y. Wang, R. Bouchard, R. S. Eagleson, P.-O. Martin, and W. R. Tyson, "Ring Hoop Tension Test (RHTT): A Test for Transverse Tensile Properties of Tubular Materials," *J. Test. Eval.*, vol. 30, pp. 382–391, 2002. https://doi.org/10.1520/JTE12328J

[17] F. Nagase, T. Sugiyama, and T. Fuketa, "Optimized ring tensile test method and hydrogen effect on mechanical properties of zircaloy cladding in hoop direction," *J. Nucl. Sci. Technol.*, vol. 46, no. 6, pp. 545–552, 2009. https://doi.org/10.1080/18811248.2007.9711560

[18] I. Barsoum and K. F. Al Ali, "A procedure to determine the tangential true stress-strain behavior of pipes," *Int. J. Press. Vessel. Pip.*, vol. 128, no. August, pp. 59–68, 2015. https://doi.org/10.1016/j.ijpvp.2014.11.002

[19] J. P. Rouse, M. Simonelli, and C. J. Hyde, "On the use of small ring testing for the characterisation of elastic and yield material property variation in additively manufactured materials," *Addit. Manuf.*, vol. 36, p. 101589, Dec. 2020. https://doi.org/10.1016/J.ADDMA.2020.101589

[20] T. M. A. A. El-Bagory, M. Y. A. Younan, and I. M. Alarifi, "Failure analysis of ring hoop tension test (RHTT) specimen under different loading conditions," *Am. Soc. Mech. Eng. Press. Vessel. Pip. Div. PVP*, vol. 3A, 2018. https://doi.org/10.1115/PVP2018-84198

[21] ASTM International, "ASTM D2290-19a, Standard Test Method for Apparent Hoop Tensile Strength of Plastic or Reinforced Plastic Pipe," *West Conshohocken, PA*, 2019. https://doi.org/10.1520/D2290-19A

[22] S.-K. Kim, J.-G. Bang, D.-H. Kim, et al., "Hoop strength and ductility evaluation of irradiated fuel cladding," *Nucl. Eng. Des. - NUCL ENG DES*, vol. 239, pp. 254–260, Feb. 2009. https://doi.org/10.1016/j.nucengdes.2008.10.024

[23] J. Desquines, D. A. Koss, A. T. Motta, B. Cazalis, and M. Petit, "The issue of stress state during mechanical tests to assess cladding performance during a reactivity-initiated accident (RIA)," *J. Nucl. Mater.*, vol. 412, no. 2, pp. 250–267, 2011. https://doi.org/10.1016/j.jnucmat.2011.03.015

[24] International Organization for Standardization, "ISO 8496, Metallic materials — Tube — Ring tensile test," 2013.

[25] S. Arsene and J. Bai, "A new approach to measuring transverse properties of structural tubing by a ring test," *J. Test. Eval.*, vol. 24, no.

6, pp. 386–391, 1996. https://doi.org/10.1520/JTE11461J

[26] S. Arsene and J. Bai, “A new approach to measuring transverse properties of structural tubing by a ring test—experimental investigation,” *J. Test. Eval.*, vol. 26, no. 1, pp. 26–30, 1998. https://doi.org/10.1520/JTE11966J

[27] E. J. Walsh and D. O. Adams, “Development and evaluation of the quadrant ring test method,” *Exp. Mech.*, vol. 48, no. 3, pp. 319–326, 2008. https://doi.org/10.1007/s11340-007-9089-x

[28] M. A. Martín-Rengel, F. J. Gómez Sánchez, J. Ruiz-Hervías, L. Caballero, and A. Valiente, “Revisiting the method to obtain the mechanical properties of hydrided fuel cladding in the hoop direction,” *J. Nucl. Mater.*, vol. 429, no. 1–3, pp. 276–283, Oct. 2012. https://doi.org/10.1016/j.jnucmat.2012.06.003

[29] J. Kazakeviciute, J. P. Rouse, D. S. A. De Focatiis, and C. J. Hyde, “The development of a novel technique for small ring specimen tensile testing,” *Theor. Appl. Fract. Mech.*, vol. 99, no. December 2018, pp. 131–139, 2019. https://doi.org/10.1016/j.tafmec.2018.11.016

[30] M. Saber and B. Ali, “On the Determination of Material Mechanical Properties of St 37 Steel Pipes Using O-Ring Specimens,” *Experimental Techniques*, vol. 45, no. 6. pp. 759–768, 2021. https://doi.org/10.1007/s40799-021-00455-3

[31] A. P. Boresi and R. J. Schmidt, *Advanced mechanics of materials*, 6th ed., vol. 117. New Jersey: John Wiley & Sons, 2003.

[32] M. G. S. Ferreira, R. Li, J. S. Fernandes, et al., “Pitting corrosion of laser surface modified aluminium alloys,” *Mater. Sci. Forum*, vol. 192–194, no. pt 1, pp. 421–432, 1995. https://doi.org/10.4028/www.scientific.net/msf.192-194.421

[33] M. Yazdani, M. R. Toroghinejad, and S. M. Hashemi, “Investigation of Microstructure and Mechanical Properties of St37 Steel-Ck60 Steel Joints by Explosive Cladding,” *J. Mater. Eng. Perform.*, vol. 24, no. 10, pp. 4032–4043, 2015. https://doi.org/10.1007/s11665-015-1670-3

[34] T. Siagian, I. Siregar, and H. Lubis, “Characteristics of St.37 Steel Materials with Temperature and Time on Heat Treatment Test using Furnace,” *Int. J. Innov. Sci. Res. Technol.*, vol. 3, no. 4, 2018.

[35] K. A. S. Hibbit, “ABAQUS/standard version 6.6, theory, example problem and user’s manuals,” *ABAQUS Inc., Rhode Isl. USA*, 2006.